JOURNAL OF Materials CHEMISTRY

Low temperature alloying of Cu and Ni nanoparticles formed within thermally evaporated fatty acid films

Chinmay Damle and Murali Sastry*

Materials Chemistry Division, National Chemical Laboratory, Pune 411 008, India.
E-mail: sastry@ems.ncl.res.in; Tel: +91 20 5893044; Fax: +91 20 5893952/5893044

Received 28th January 2002, Accepted 2nd April 2002
First published as an Advance Article on the web 26th April 2002

The low temperature alloying of copper and nickel nanoparticles synthesized in a fatty acid film by a novel ion-entrapment process is described. Nanoparticles of copper and nickel were grown in thermally evaporated stearic acid films by immersion of the film sequentially in solutions containing Cu^{2+} ions and Ni^{2+} ions followed by their *in-situ* reduction at each stage. Entrapment of Cu^{2+} and Ni^{2+} ions in the stearic acid film occurs by selective electrostatic binding with carboxylate ions in the fatty acid matrix. Thermal treatment of the stearic acid–(Cu + Ni) nanocomposite film at 100 °C resulted in the formation of a Cu–Ni alloy. The process of Cu^{2+} and Ni^{2+} ion incorporation in the stearic acid matrix and synthesis of the Cu–Ni alloy were followed by quartz crystal microgravimetry (QCM), Fourier transform infrared (FTIR) spectroscopy, transmission electron microscopy (TEM) and X-ray diffraction (XRD).

Introduction

During the last decade, the area of nanotechnology has witnessed increased scientific interest due to the fact that the catalytic, mechanical, electronic, optical, and other properties of a material are significantly altered at nanoscale dimensions.[1] One of the main challenges in the field of nanotechnology where there is great scope for experimentation is the synthesis of nanoparticles in different hosts to yield nanocomposite materials. A number of different templates have been used for the synthesis of nanoparticles such as polymers,[2] porous glasses,[3] zeolites and mesoporous silica,[4] phospholipid membranes,[5] inverse microemulsions,[6] poly(amidoamine) dendrimers,[7] self-assembled monolayers[8] as well as bio-templates such as self-assembled bacterial S-layers[9] and the tobacco mosaic virus (TMV).[10] One of the more thoroughly studied methods for the growth of nanoparticles has been based on the use of Langmuir–Blodgett (LB) films of metal salts of fatty acids. This 'insertion chemistry' approach to the *in-situ* generation of nanoparticles of metals,[11] semiconductors[12] and oxides[13] in LB films has received much attention over the last decade.

In this laboratory, we have demonstrated the spontaneous self-organization of thermally evaporated fatty acid films during immersion in electrolyte solutions such as $PbCl_2$ and $CdCl_2$ leading to the formation of *c*-axis oriented films of metals salts of fatty acids very similar to the lamellar structures obtained by the LB technique.[14] As a part of our ongoing studies in the use of thermally evaporated lipid films in the entrapment of ions,[14] surface-modified colloidal particles,[15] proteins/enzymes[16] and DNA/PNA (peptide nucleic acids, DNA mimics),[17] we demonstrate herein the incorporation of Cu^{2+} and Ni^{2+} ions in thermally evaporated stearic acid (StA) films by a simple beaker-based immersion protocol as well as the reduction of the metal ions *in-situ* to form metal nanoparticles, wherein the low-temperature annealing results in the formation of a nanoscale alloy. We have recently used this technique in the patterned assembly of gold[18] and CdS nanoparticles assemblies.[19] At this point, we would like to highlight an important difference between the use of LB films to obtain nanoparticle assemblies[11–13] and our method based on the use of thermally evaporated lipid films—the use of thermally evaporated lipid films enables the generation of patterned structures for different applications while such patterned structures are not realizable by the LB technique. This technique can thus be conveniently used to synthesize a combination/variety of alloys by patterning a single template, which cannot be achieved in principle by other conventional techniques employed to synthesize nanoscale alloys. These nanoalloys can be affectively used as a surface coating and also for various optoelectronic and catalytic applications. This is the first demonstration of hetero-nanoparticle formation *within the same lipid matrix* by the ion/biomacromolecule-entrapment method developed in this laboratory.[14,17–19] The procedure is extremely simple and consists of the steps illustrated in Scheme 1. In the first step, the thermally evaporated StA film is immersed in $CuSO_4$ solution and Cu^{2+} ions incorporated into the acid film. The metal ions are then reduced with hydrazine vapor to yield copper particles in the fatty acid matrix. This process regenerates free carboxylic acid groups that may be used to incorporate Ni^{2+} ions during immersion in $NiSO_4$ solution. Another cycle of reduction of this film with hydrazine results in the formation of Ni nanoparticles co-existing with the

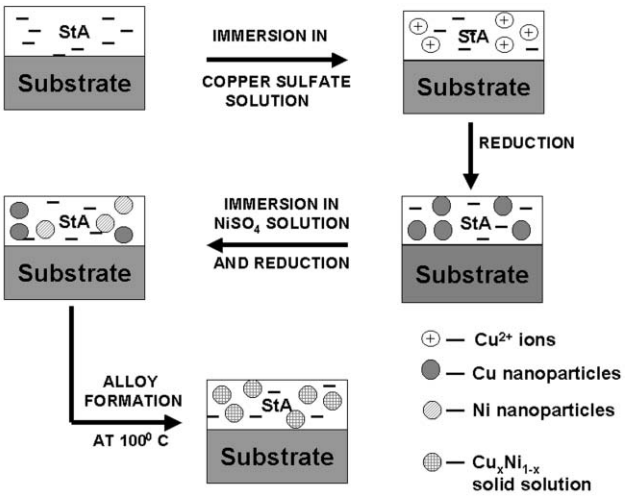

Scheme 1 Diagram illustrating the various steps involved in the preparation of the StA–(Cu + Ni) nanoparticle film and the *in-situ* nanoscale alloying.

 DOI: 10.1039/b201026g

previously formed copper particles. Thermal treatment of the StA–(Cu+Ni) nanocomposite film indicated the formation of a Cu–Ni alloy at 100 °C. It is well known that Cu and Ni are soluble in the liquid as well as the solid state,[20] the alloy formation taking place essentially above 1000 °C in the bulk state.[20] Nanocrystalline Cu–Ni alloy has been synthesized earlier using mechanical alloying[21] and by laser ablating targets prepared by cold-pressing powder mixtures of Cu and Ni,[22] the temperature of alloying being very high in these cases as well. In this study, alloy formation from Cu and Ni nanoparticles occurs at the comparatively low temperature of 100 °C and is a salient result of this investigation. The kinetics (and extent) of metal ion incorporation has been followed by quartz crystal microgravimetry (QCM) while the formation of the metal salt of StA was studied using Fourier transform infrared (FTIR) spectroscopy. The formation of Cu and Ni nanoparticles and their low-temperature alloying were studied by X-ray diffraction (XRD) and transmission electron microscopy (TEM) measurements. Presented below are details of the investigation.

Experimental details

Thin films of stearic acid (500 Å thickness) were thermally vacuum deposited in an Edwards E306 vacuum coating unit operated at a pressure of 1×10^{-7} Torr onto carbon-coated TEM grids, gold-coated AT-cut quartz crystals for QCM measurements and Si (111) substrates for FTIR and XRD measurements. The film thickness and deposition rate were monitored *in-situ* using an Edwards QCM. The kinetics of incorporation of Cu^{2+} ions into the stearic acid films was followed by measurement of the change in resonance frequency of the stearic acid covered QCM crystal during immersion in 10^{-4} M aqueous $CuSO_4$ solution. The pH of the electrolyte was adjusted to 6 so that complete ionization of the carboxylic acid groups would occur thereby leading to maximum loading of the fatty lipid films with the copper ions. The frequency measurements were made *ex-situ* on an Edwards FTM5 frequency counter (stability and resolution of 1 Hz) after thorough washing of the crystals with deionized water and drying in flowing N_2. For the 6 MHz crystal used in this study, the mass resolution was 12.1 ng cm^{-2} and the frequency changes were converted to mass loading using the Sauerbrey equation.[23]

The optimum immersion time determined from the QCM kinetics measurements was used to load the stearic acid films on Si (111) substrates with Cu^{2+} ions by similar immersion in 10^{-4} M $CuSO_4$ solution. After formation of copper stearate films, the films on Si (111) substrates were subjected to FTIR and XRD analysis. FTIR measurements were carried out in the diffuse reflectance mode at a resolution of 4 cm^{-1} on a Shimadzu FTIR-8201 PC instrument while XRD studies were carried out in the transmission mode on a Philips PW 1830 instrument operating at 40 kV voltage and a current of 30 mA with Cu K_α radiation. Thereafter, the copper stearate coated QCM crystal and Si substrates were kept in an atmosphere of hydrazine to reduce the copper ions in the lipid film. After hydrazine treatment (which required typically 2 hours), it was observed that there was a small increase in the mass of the copper stearate film on the QCM crystal that was attributed to trapped hydrazine in the film. Gentle heating at *ca.* 50 °C for 15 min resulted in removal of the trapped hydrazine and restoration of the film mass to the value measured at the start of the hydrazine treatment. This heat treatment was given before each successive cycle of ion-exchange and reduction. The reduced films on Si substrates were analyzed by FTIR, XRD and TEM. TEM measurements were carried out on a JEOL Model 1200EX instrument operated at an accelerating voltage of 120 kV. The nanoparticle films for TEM analysis were prepared by immersing the TEM grids in chloroform for 15 minutes in order to dissolve the lipid matrix and has previously been shown to lead to close-packing of the nanoparticles.[24]

On completion of the first cycle of Cu^{2+} incorporation and reduction, QCM measurements of the kinetics of Ni^{2+} incorporation in the StA–Cu nano film were performed by immersion of this film in 10^{-4} M $NiSO_4$ solution and monitoring *ex-situ* the frequency changes of the quartz crystal. On completion of the Ni^{2+} ion exchange cycle, the ions were reduced with hydrazine in a manner similar to that adopted for the copper stearate film and the films analyzed by FTIR and XRD measurements. It was observed that the extent of Ni^{2+} incorporation in the films was much smaller than that of Cu^{2+} ions and therefore, two additional cycles of Ni^{2+} exchange and reduction were required before a measurable signal from the Ni nanoparticles (the (111) Bragg reflection from Ni at a 2θ value of 44° was used an indicator) could be observed. The size of the copper and nickel particles in the film were estimated from the line-width broadening of the (111) Bragg reflections using the Debye–Scherrer formula.[25]

The thermal stability of the StA–(Cu + Ni) nanoparticle film and the formation of a Cu–Ni alloy were studied by heating the film to different temperatures and following changes in the XRD patterns. The films were heated at 50 °C and 75 °C for one hour and finally at 100 °C for 1 hour.

Results and discussion

The kinetics of incorporation of Cu^{2+} and Ni^{2+} ions into a 500 Å thick StA film was followed by QCM and the data obtained are shown in Fig. 1. The individual cycles of mass exchange are clearly indicated in the figure next to the respective curves. The first cycle of Cu^{2+} incorporation into the film on immersion in 10^{-4} M $CuSO_4$ solution (pH = 6) resulted in a mass uptake of *ca.* 41000 ng cm^{-2}. From the mass of StA deposited onto the quartz crystal (*ca.* 2220 ng cm^{-2}) it can be easily shown that the Cu^{2+} ion : StA ratio works out to nearly 80 : 1. This result indicates a high degree of overcompensation of the charge in the StA film by the Cu^{2+} ions. It may be mentioned that such charge overcompensation is known to occur during complexation of macroions such as phosphotungstate anions with fatty amine Langmuir monolayers at the air–water interface[26] and is also the mechanism by which layer-by-layer electrostatic assembly occurs on planar surfaces.[27] However the degree of charge overcompensation in this study is very large and not understood at this time. This result was reproducible and it was found that the mass uptake curves in separate runs agreed to within 5%.

After reduction of the copper stearate film by a 2 hour hydrazine treatment, the QCM crystal was further immersed in

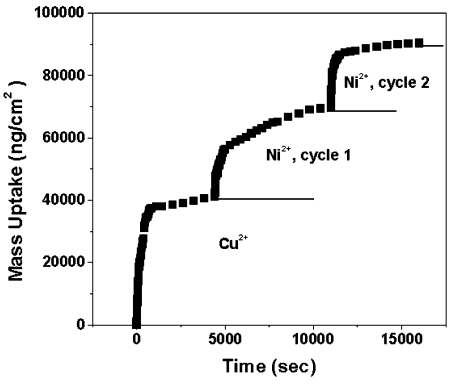

Fig. 1 QCM mass uptake recorded *ex-situ* during Cu^{2+} and Ni^{2+} ion incorporation in a 500 Å thick thermally evaporated StA film (see text for details). The different cycles of ion exchange are indicated next to the respective curves.

$NiSO_4$ solution (10^{-4} M, pH = 6) and the Ni^{2+} QCM mass uptake recorded during this first cycle of immersion is shown in Fig. 1. The final mass uptake during this cycle of ion exchange yielded a value of *ca.* 29000 ng cm^{-2} and results in a *ca.* 1.3 : 1 Cu^{2} : Ni^{2+} mass ratio. Similarly, one more cycle of reduction and Ni^{2+} incorporation in the StA films was carried out and the QCM mass uptake data for this cycle are also shown in Fig. 1. In the second cycle of Ni^{2+} ion uptake, the final mass loading was 21600 ng cm^{-2}. This value corresponds to a Cu^{2+} : Ni^{2+} mass ratio of 1.8 : 1 (for the second cycle alone). Thus, the overall Cu^{2+} : Ni^{2+} molar ratio at the end of one cycle of Cu^{2+} incorporation and two cycles of Ni^{2+} incorporation may be easily shown to be *ca.* 1 : 1.3. As mentioned earlier, reduction of the metal ions leads to regeneration of free carboxylic acid groups in the lipid matrix thus facilitating further ion exchange.

The formation of the metal salts of stearic acid and reduction of the electrostatically entrapped Cu^{2+} and Ni^{2+} ions in the StA matrix is conveniently followed by FTIR measurements. Fig. 2 shows the FTIR spectra recorded in the range 1400–1900 cm^{-1} for a 500 Å thick StA film deposited on a Si (111) wafer after various cycles of ion exchange and reduction. Curve 1 in the figure represents the spectrum recorded from the as-deposited StA film on Si. A number of prominent features are seen, the most germane to this study being the resonances at 1700 cm^{-1} and 1460 cm^{-1} which are assigned to the carbonyl stretch[14,28] and methylene scissoring[14,29–30] motions respectively. We would like to point out that a single peak is seen at 1460 cm^{-1} and this indicates that the hydrocarbon chains in the StA matrix are in a rather disordered state.[14,29,30] The FTIR spectrum recorded from the StA film after one cycle of Cu^{2+} incorporation is shown as curve 2 in Fig. 2. It is observed that on formation of the copper salt of stearic acid, the carbonyl stretch frequency shifts from 1700 cm^{-1} to *ca.* 1580 cm^{-1} clearly indicating the binding of the Cu^{2+} ions with the carboxylate ions of StA. The shift in the carbonyl stretch frequency to lower wavenumbers followed by the disappearance of the 1700 cm^{-1} resonance is known to be a clear indicator of salt formation in such fatty acid films[14,28] and indicates in this case complete copper stearate salt formation.

Reduction of the Cu^{2+} ions in the copper stearate film followed by incorporation of Ni^{2+} ions resulted in the FTIR spectrum shown as curve 3 in Fig. 2. It is observed that the methylene scissoring band is considerably reduced in intensity and the carbonyl stretch band now appears as a broad resonance centered at *ca.* 1670 cm^{-1}. The former result indicates that the hydrocarbon chains in the StA molecules are considerably disordered on formation of the copper nanoparticles and is likely to be due to surface coordination of the stearic acid molecules with the copper nanoparticles generated *in-situ*. It is known that fatty acid molecules bind to the surface of colloidal silver[31] and we believe that in the case of copper particles generated within the fatty acid matrix, significant distortion to the lamellar, bilayer structure would occur *via* binding of the nanoparticles with the fatty acid molecules. As will be seen below, this inference is also in agreement with XRD data of the StA–Cu nano film. The presence of a broad band at 1670 cm^{-1} and not complete reappearance of the 1700 cm^{-1} band upon reduction of the Cu ions indicates weak binding of the stearate ions with the Cu nanoparticle surface. Curve 4 in Fig. 2 represents the FTIR spectrum recorded from the film shown as curve 3 after two cycles of Ni^{2+} ion exchange. The shift in the carbonyl stretch resonance to 1530 cm^{-1} indicates the binding of the Ni^{2+} ions with the carboxylate ions in the StA matrix and thus, formation of the nickel stearate salt. Curve 5 in Fig. 2 represents the FTIR spectrum recorded after reduction of the Ni^{2+} ions in the film shown in curve 4. The curve is essentially featureless indicative of complete formation of Cu and Ni nanoparticles within the acid film. The absence of any band at 1700 cm^{-1} suggests the binding of free carboxylic acid groups with the metal nanoparticles.

The transmission electron micrograph recorded from a 500 Å thick StA film after one cycle of Cu^{2+} and Ni^{2+} ion exchange and subsequent reduction with hydrazine is shown in Fig. 3A. The StA matrix was removed from this composite film by soaking the film in chloroform for 15 minutes and carefully removing the TEM grid from the organic phase. A number of well-dispersed particles can clearly be seen in the TEM picture with a fairly even size distribution. The particle size histogram for this micrograph is plotted in Fig. 3B. While the individual copper and nickel nanoparticles cannot be distinguished from the TEM picture, an average size of 350 Å was estimated for the ensemble of nanoparticles in the TEM picture.

XRD patterns recorded from a 500 Å thick StA film under different stages of ion exchange and reduction are shown in Fig. 4. Fig. 4A shows the XRD patterns recorded from the StA film after the first cycle of Cu^{2+} ion incorporation (curve 1) and after *in-situ* reduction of the copper ions to form copper nanoparticles (curve 2). It is seen that the copper stearate film shows a *c*-axis oriented lamellar structure and a number of (00*l*) Bragg reflections are indexed in Fig. 4A. From the 2θ values of the 5 Bragg reflections observed for this film, a *d*-spacing of 48.9 Å is calculated. This value is in good agreement with the expected *d*-spacing based on the length of the StA molecule and the size of the Cu^{2+} ion[32] and clearly shows the presence of an ordered, lamellar phase with the hydrocarbon chains of the StA molecules in the all-*trans* packing configuration. Please also

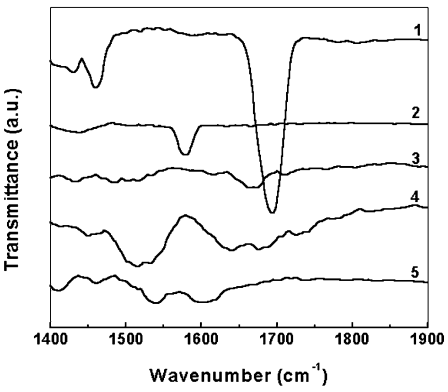

Fig. 2 FTIR spectra recorded from a 500 Å thick StA film deposited on a Si (111) substrate (curve 1); the StA film shown as curve 1 after incorporation of Cu^{2+} ions (curve 2); the StA film shown as curve 2 after reduction of the copper ions (curve 3); the StA film shown as curve 3 after two cycles of Ni^{2+} exchange (curve 4); the StA film shown as curve 4 after reduction of the nickel ions (curve 5).

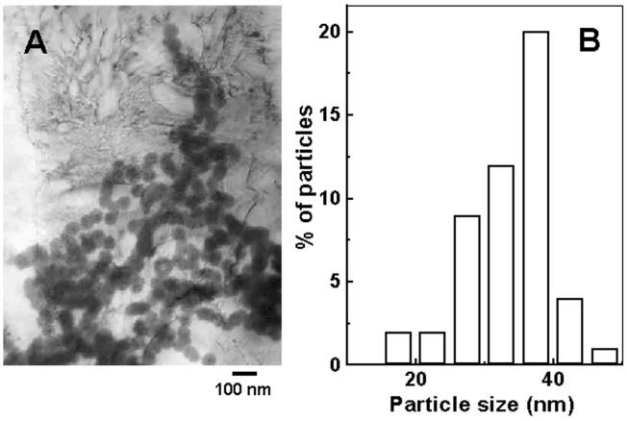

Fig. 3 A) TEM picture recorded from a 500 Å thick StA film after one cycle of Cu^{2+} and Ni^{+} ion incorporation and reduction. The lipid matrix was removed by soaking the StA–(Cu + Ni) nanocomposite film in chloroform for 15 min. B) Particle size distribution histogram of the Cu and Ni nanoparticles shown in Fig. 3A.

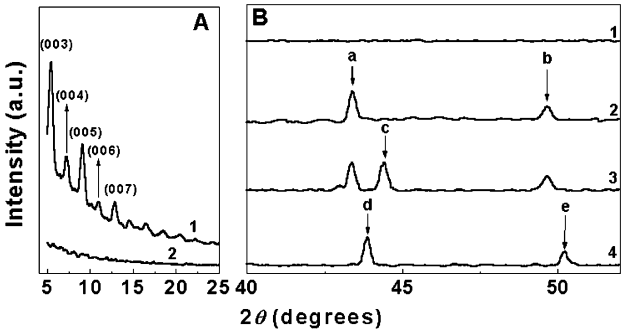

Fig. 4 A) XRD pattern recorded from a 500 Å thick StA film after incorporation of Cu^{2+} ions (curve 1) and the copper stearate film after reduction of the copper ions by hydrazine treatment to form copper nanoparticles (curve 2). The (00*l*) Bragg reflections are indexed in the figure. B) XRD patterns in the range of the (111) Bragg reflections from Cu (features a and b), Ni (feature c) and the Cu–Ni alloy (features d and e) recorded from a 500 Å thick StA film after immersion in Cu^{2+} ion solution (curve 1); film shown as curve 1 after reduction of the copper ions (curve 2); film shown as curve 2 after two cycles of Ni^{2+} incorporation and reduction of the nickel ions (curve 3); film shown as curve 3 after heating at 100 °C for 1 h (curve 4).

note the characteristic odd–even intensity oscillations in the (00*l*) Bragg reflections from the copper stearate film (curve 1, Fig. 4A). This intensity oscillation has been shown to be a consequence of lamellar ordering of films of fatty acid salts[32] and is, in some sense, an indicator of the packing of the hydrocarbon chains in the film. On reduction of the copper ions to form copper nanoparticles, the lamellar ordering in the film vanishes as evidenced by the disappearance of the (00*l*) Bragg reflections (curve 2, Fig. 4A) The fact that incorporation of Ni^{2+} ions after the reduction of Cu ions does not lead to restoration of lamellar order in the films (curve 2, Fig. 4A) indicates that the distortion to the bilayer structure on formation of the copper nanoparticles is quite large and suggests a significant density of large copper particles in the film.

Fig. 4B shows XRD patterns recorded from a 500 Å thick StA film after the first cycle of Cu^{2+} incorporation (curve 1); the film shown as curve 1 after reduction of the copper ions (curve 2); the film shown as curve 2 after two cycles of Ni^{2+} incorporation and reduction (curve 3) and the film shown as curve 3 after heating at 100 °C for 1 h (curve 4). A number of features labeled a–e have been identified in the figure and are located at 2θ values of 43.2°, 49.7°, 44.4°, 43.9° and 50.2° respectively. While the copper stearate film is essentially featureless in the 2θ range 40–55° (Fig. 4B, curve 1), reduction of the copper ions by hydrazine treatment leads to the growth of the (111) and (200) Bragg reflections at 2θ values of 43.2° and 49.7° respectively from the copper nanoparticles generated *in-situ* (Fig. 4B, curve 2, features a and b). The size of the copper nanoparticles in this film was calculated from the broadening of the (111) reflection using the Debye–Scherrer formula to be *ca.* 160 Å. We recollect that a very large mass uptake was observed for both Cu^{2+} and Ni^{2+} ions in the StA film and may be responsible for the large particles observed in this study. It should be possible, in principle, to limit the degree of salt formation and, consequently, the size of the nanoparticles grown in thermally evaporated lipid films and this is an aspect we are currently exploring.

The XRD pattern recorded from the reduced copper stearate film after two cycles of Ni^{2+} ion incorporation and reduction is represented as curve 3, Fig. 4B. An additional peak at a 2θ value of 44.4° is clearly seen in this diffraction pattern (feature c) and arises due to the (111) Bragg reflection from the Ni particles grown in the StA matrix. The size of the nickel particles was calculated from the broadening of the (111) Bragg reflection (feature c) to be *ca.* 180 Å and, like the copper particles, the Ni nanoparticles are large. The underestimation of the size of Cu and Ni nanoparticles by XRD analysis in comparison with the TEM estimate (Fig. 3) may be due to uncertainties in the fitting procedure/experimental errors in the XRD line-broadening analysis. Even though the Cu and Ni particles are well within nanoscale dimensions, we term the particles 'large' since their dimensions are much in excess of the thickness of the StA bilayers (*ca.* 50 Å) in which they are embedded. There was no significant change in the size of the copper particles after formation of Ni nanoparticles indicating that the nickel particles nucleate and grow separately.

The StA–(Cu + Ni)-nano film was heated at 100 °C for 1 h and the XRD pattern obtained after this thermal treatment is represented by curve 4, Fig. 4B. Two new Bragg reflections at 2θ values of 43.9° and 50.2° are observed from this film and are assigned to the (111) and (200) Bragg reflections respectively from the Cu_xNi_{1-x} alloy phase with an fcc structure and a lattice parameter in between those of Cu and Ni. These peaks agree well with those reported in the literature for laser-ablated films of Cu–Ni powder pressed targets.[22] Considering the Vegard's law behavior for the Cu–Ni system,[22] the composition of the solid solution can be calculated from the position of the (111) Bragg reflection of the alloy phase (2θ = 43.7°) to be $Cu_{0.5}Ni_{0.5}$. This result is in good agreement with the Cu : Ni ratio of *ca.* 1 : 1.3 in the StA films calculated from the QCM data (Fig. 1). Prior to the thermal treatment at 100 °C, we had measured the XRD spectra from StA–(Cu + Ni)-nano films heated at 50 °C and 75 °C for 1 h and did not notice any changes associated with the formation of an alloy phase. Thus, aggregation of the copper and nickel particles occurs at 100 °C leading to the formation of a Cu_xNi_{1-x} alloy phase (curve 4, Fig. 4B). To the best of our knowledge, lowering of temperature to such an extent to form a nanoscale Cu_xNi_{1-x} alloy phase has hitherto never been observed. This may be a consequence of the fact that StA melts at close to 80 °C and heating to 100 °C thus provides sufficient mobility to the Cu and Ni particles to diffuse within the StA matrix and form the Cu–Ni alloy phase. This result suggests that the high surface free energy of the metal in nanoparticle form is, to a large extent, responsible for this considerable lowering of the annealing temperature. It may also be possible that the StA matrix plays a role in the lowering of the alloy formation temperature and is another aspect that requires further investigation.

In conclusion, the formation of copper and nickel nanoparticles in thermally evaporated stearic acid films by a process of ion exchange and reduction has been demonstrated. The copper and nickel particles could be grown simultaneously in the fatty acid matrix and a low temperature heat treatment of the nanoparticle film at 100 °C resulted in the formation of a Cu–Ni alloy phase. This is a salient result of the investigation, such alloy formation is normally reported to occur at much higher temperatures. Efforts are underway to control the size of the nanoparticles grown by this route and to investigate other binary alloy combinations. The main advantage of the use of thermally evaporated lipid films in the formation of fatty acid metal salts as precursors to nanoalloy formation over the conventional LB method is that patterned structures may be readily obtained by suitable masking thereby adding an additional degree of freedom. In addition to the nanoscale alloying demonstrated herein, we have used such patterned thermally evaporated lipid films in DNA detection[17a] and in the generation of multi-enzyme films.[16d] The low temperature alloying of the nanoparticles demonstrated in this paper coupled with the patterning of the template to synthesize various binary nanoscale alloys on a single surface gives this technique an added advantage over other conventional methods. Our future course of action would be to study the simultaneous incorporation of two or more metal ions in the lipid films and their *in-situ* reduction. Since the assembly of metal ions in this case occurs at a molecular level, we believe

this could result in room temperature alloying, which is currently not achievable by any other technique.

Acknowledgement

This work was partially funded by a grant from the Indo-French Center for the Promotion of Advanced Scientific Research (IFCPAR), New Delhi and is gratefully acknowledged. TEM measurements were carried out by Mr. Rajesh Gonnade, Materials Chemistry Division, NCL Pune, and is gratefully acknowledged.

References

1 The interested reader is referred to the recent Feb. 28, 2000 issue of *Chem. Eng. News* and the articles by R. Dagani for coverage of the applications envisaged for nanomaterials.
2 L. L. Beecoft and C. K. Ober, *Chem. Mater.*, 1997, **9**, 1302.
3 B. L. Justus, R. J. Tonnucci and A. D. Berry, *Appl. Phys. Lett.*, 1992, **61**, 3151.
4 (*a*) Y. Wang and N. J. Herron, *J. Phys. Chem.*, 1988, **92**, 4988; (*b*) P. Mukherjee, C. Patra, R. Kumar and M. Sastry, *PhysChemComm*, 2001, **5**.
5 X. K. Zhao, S. Barai, R. Rolandi and J. H. Fendler, *J. Am. Chem. Soc.*, 1988, **110**, 1012.
6 P. A. Dresco, V. S. Zaitsev, R. J. Gambino and B. Chu, *Langmuir*, 1999, **15**, 1945.
7 M. E. Garcia, L. A. Baker and R. M. Crooks, *Anal. Chem.*, 1999, **71**, 256.
8 V. Patil, K. S. Mayya and M. Sastry, *J. Mater. Sci. Lett.*, 1997, **16**, 899.
9 (*a*) W. Shenton, D. Pum, U. B. Sleytr and S. Mann, *Nature*, 1997, **389**, 585; (*b*) U. B. Sleytr, P. Messner, D. Pum and M. Sara, *Angew. Chem., Int. Ed.*, 1999, **38**, 1034.
10 W. Shenton, T. Douglas, M. Young, G. Stubbs and S. Mann, *Adv. Mater.*, 1999, **11**, 253.
11 (*a*) A. T. Ruadel, J. Leloup and A. Barraud, *Mol. Cryst. Liq. Cryst.*, 1986, **134**, 347; (*b*) K. C. Yi, Z. Horvolgyi and J. H. Fendler, *J. Phys. Chem.*, 1994, **98**, 3872; (*c*) S. X. Ji, C. Y. Fan, F. Y. Ma, X. C. Chen and L. Jiang, *Thin Solid Films*, 1994, **242**, 16; (*d*) F. C. Meldrum, N. A. Kotov and J. H. Fendler, *Langmuir*, 1994, **10**, 2035.
12 (*a*) J. Yang, F. C. Meldrum and J. H. Fendler, *J. Phys. Chem.*, 1995, **99**, 5500; (*b*) J. Yang and J. H. Fendler, *J. Phys. Chem.*, 1995, **99**, 5505; (*c*) D. J. Elliot, D. N. Furlong, T. R. Gegenbach, F. Grieser, R. S. Urquhart, C. L. Hoffman and J. F. Rabolt, *Colloids Surf. A*, 1995, **103**, 207; (*d*) R. S. Urquhart, D. N. Furlong, T. Gegenbach, N. J. Geddes and F. Grieser, *Langmuir*, 1995, **11**, 1127.
13 (*a*) D. M. Taylor and J. N. Lambi, *Thin Solid Films*, 1994, **243**, 384; (*b*) D. V. Paranjape, M. Sastry and P. Ganguly, *Appl. Phys. Lett.*, 1993, **63**, 18; (*c*) D. T. Amm, D. J. Johnson, Y. Laursen and S. K. Gupta, *Appl. Phys. Lett.*, 1992, **61**, 522.
14 P. Ganguly, S. Pal, M. Sastry and M. N. Shashikala, *Langmuir*, 1995, **11**, 1078.
15 (*a*) M. Sastry, *Handbook of Surfaces and Interfaces of Materials*, ed. H. S. Nalwa, Academic Press, 2001, vol. 3, ch. 2, p. 88 and references therein; (*b*) M. Sastry, *Curr. Sci.*, 2000, **78**, 1089.
16 (*a*) A. Gole, C. V. Dash, M. Rao and M. Sastry, *Chem. Commun.*, 2000, 297; (*b*) A. Gole, C. V. Dash, A. B. Mandale, M. Rao and M. Sastry, *Anal. Chem.*, 2000, **72**, 1401; (*c*) S. Mandal, A. Gole, N. Lala and M. Sastry, *Langmuir*, 2001, **17**, 6262; (*d*) A. Gole and M. Sastry, *Biotechnol. Bioeng.*, 2001, **74**, 172.
17 (*a*) M. Sastry, V. Ramakrishnan, M. Pattarkine and K. N. Ganesh, *J. Phys. Chem. B*, 2001, **105**, 4409; (*b*) V. Ramakrishnan, M. Sable, M. D'Costa, K. N. Ganesh and M. Sastry, *Chem. Commun.*, 2001, 2622.
18 S. Mandal, S. R. Sainkar and M. Sastry, *Nanotechnology*, 2001, **12**, 1.
19 S. Mandal, C. Damle, S. R. Sainkar and M. Sastry, *J. Nanosci. Nanotechnol.*, 2001, **1**, 281.
20 T. B. Massalki, H. Okamoto and P. R. Subramanian, *Binary alloy phase diagrams*, 2nd edition, ASM International, Metals Park, OH, 1990.
21 S. K. Pabi, J. Joardar, I. Manna and B. S. Murty, *Nanostruct. Mater.*, 1997, **9**, 149.
22 R. P. van Ingen, R. H. J. Fastenau and E. J. Mittenmeijer, *J. Appl. Phys.*, 1994, **76**, 1871.
23 G. Sauerbrey, *Z. Phys. (Munich)*, 1959, **155**, 206.
24 V. Patil and M. Sastry, *Langmuir*, 2000, **16**, 2207.
25 J. W. Jeffrey, *Methods in Crystallography*, Academic Press, New York, 1971.
26 N. Cuvillier and F. Rondelez, *Thin Solid Films*, 1998, **19**, 327.
27 G. Decher, *Science*, 1997, **277**, 1232.
28 J. F. Rabolt, F. C. Burns, N. Schlotter and J. D. Swalen, *J. Chem. Phys.*, 1983, **78**, 946.
29 R. G. Snyder, *J. Mol. Spectrosc.*, 1961, **7**, 116.
30 N. Lala and M. Sastry, *Phys. Chem. Chem. Phys.*, 2000, **2**, 2461.
31 V. Patil, K. S. Mayya, S. D. Pradhan and M. Sastry, *J. Am. Chem. Soc*, 1997, **119**, 9281.
32 P. Ganguly, D. V. Paranjape, K. R. Patil and S. K. Chaudhari, *Langmuir*, 1992, **8**, 2365.